Meteorologische Zeitschrift, Vol. **24**, No. 4, 411–423 (published online April 4, 2015)

Article

Linking teleconnection patterns to European temperature – a multiple linear regression model

Henning W. Rust[1*], Andy Richling[1], Peter Bissolli[2] and Uwe Ulbrich[1]

[1]Institute for Meteorology, Freie Universität Berlin, Berlin, Germany
[2]Deutscher Wetterdienst, Offenbach, Germany

(Manuscript received August 4, 2014; in revised form December 23, 2014; accepted January 26, 2015)

Abstract

The link between the indices of twelve atmospheric teleconnection patterns (mostly Northern Hemispheric) and gridded European temperature data is investigated by means of multiple linear regression models for each grid cell and month. Furthermore index-specific signals are calculated to estimate the contribution to temperature anomalies caused by each individual teleconnection pattern. To this extent, an observational product of monthly mean temperature (E-OBS), as well as monthly time series of teleconnection indices (CPC, NOAA) for the period 1951–2010 are evaluated. The stepwise regression approach is used to build grid cell based models for each month on the basis of the five most important teleconnection indices (NAO, EA, EAWR, SCAND, POLEUR), which are motivated by an exploratory correlation analysis. The temperature links are dominated by NAO and EA in Northern, Western, Central and South Western Europe, by EAWR during summer/autumn in Russia/Fenno-Scandia and by SCAND in Russia/Northern Europe; POLEUR shows minor effects only. In comparison to the climatological forecast, the presented linear regression models improve the temperature modelling by 30–40 % with better results in winter and spring. They can be used to model the spatial distribution and structure of observed temperature anomalies, where two to three patterns are the main contributors. As an example the estimated temperature signals induced by the teleconnection indices is shown for February 2010.

Keywords: Teleconnection Pattern, NAO, European Temperature, Linear Model, Stepwise Regression

1 Introduction

Atmospheric teleconnection patterns and the associated indices as defined by the National Oceanic and Atmospheric Administration (NOAA) reflect the large-scale variability of the atmosphere in terms of pressure or geopotential heights. As the teleconnection indices specify the strength of the associated patterns, they describe to a certain extent the state of the atmospheric circulation and thus large scale advection of temperature and moisture. The latter have a strong influence on regional weather, particularly for temperature and precipitation; a link between these teleconnection indices and local temperature is thus a valuable tool for climate monitoring, process oriented climate model validation (e.g. Maraun et al., 2012) and downscaling of climate change projections.

There are numerous studies analysing the link between European temperature (mostly winter) and Northern Hemispheric (NH) teleconnection patterns. The prominent role of the North Atlantic Oscillation (NAO) for Europe has been investigated by, e.g. Bliss and Walker (1932); Van Loon and Rogers (1978); Hurrel (1995); Hurrell and Deser (2009). The relation between the East Atlantic pattern (EA) and European temperature has been studied by Moore and Renfrew (2012); the Scandinavian pattern (SCAND, EU1 in Barnston and Livezey (1987)) affects temperatures from Central Siberia to Central Europe (Bueh and Nakamura, 2007). Links between the East Atlantic/Western Russia pattern (EAWR, EU2 in Barnston and Livezey (1987)) and Mediterranean climate are examined via analyses of the North Sea/Caspian pattern (NCP in Kutiel and Benaroch (2002)), which is a component of the EAWR pattern we are using in the presented study. Significant correlations between NCP and temperatures are found in South Eastern Europe (Kutiel and Benaroch, 2002; Kutiel et al., 2002; Ulbrich et al., 2012). While several authors note that the influence of the patterns is affecting the specific parameters and regions at the same time (e.g. Nissen et al., 2010), we have not seen a systematic approach to disentangle the individual factors for a comparative large number of such patterns.

Here, we systematically study the effect of a set of teleconnection patterns on European temperature and seek for a quantitative description of their individual contribution to temperature anomalies, we refer to these contributions as the teleconnection patterns temperature signal. The choice of patterns is motivated by a study from Barnston and Livezey (1987) who identified 10 Northern Hemispheric teleconnection patterns. Besides those, we use the Arctic Oscillation (AO) (e.g. Thompson and Wallace, 1998) and due to a poten-

*Corresponding author: Henning Rust, Institute for Meteorology, Freie Universität Berlin, Carl-Heinrich-Becker-Weg 6–10, 12165 Berlin, Germany, e-mail: henning.rust@met.fu-berlin.de

DOI 10.1127/metz/2015/0642

Gebrüder Borntraeger Science Publishers, Stuttgart, www.borntraeger-cramer.com

tial ENSO (El Niño-Southern Oscillation) influence on Europe (e.g. Pozo-Vázquez et al., 2001; Halpert and Ropelewski, 1992; Fraedrich, 1994; Van Oldenborgh et al., 2000; Knippertz et al., 2003), we include also the Southern Oscillation (SO, e.g. Walker and Bliss, 1932). A multiple linear regression model for temperature quantifies the influence of individual teleconnection patterns. The model is built with stepwise regression and an additional cross-validation step to prevent overfitting. To reduce the model building effort, we select 5 predictors out of the 12 indices based on the Pearson correlation coefficient.

The temperature dataset, as well as the teleconnection patterns are described in Section 2 together with a brief review on stepwise multiple linear regression. Section 3 describes the regression model building, i.e. results of the predictor pre-selection (Section 3.1) and the set up of the linear model for linking teleconnection patterns to temperatures (Section 3.2). An exemplifying set of temperature signals is discussed in Section 3.3. Finally, we assess the model performance in terms of the MSE skill score (Section 3.4). A summary and discussion in Section 4 conclude this paper.

2 Data and methods

2.1 Data

2.1.1 E-OBS gridded temperature

With the E-OBS dataset (version 6) the European Climate Assessment & Dataset project (ECA&D) provides a gridded dataset with daily mean temperatures for Europe for the period from 1951 to 2010. This dataset is based on interpolated station data from providers in the ECA&D project, described in detail by Haylock et al. (2008). We selected the dataset defined on a regular geodetic grid with $0.5° \times 0.5°$ in the Euro-Atlantic region bounded by $40.25°$ W, $75.25°$ E; $25.25°$ N, $75.25°$ N and calculated monthly mean temperatures. Note, that station density and available time periods are heterogeneous; especially in Northern Africa the density is quite low and there is a reduced time period of basically 38 years (16 years in the central region of Egypt) available only. Typically, more observations have been incorporated into the dataset towards the end of the time period.

2.1.2 Teleconnection patterns

Ten Northern Hemispheric teleconnection patterns have been identified by Barnston and Livezey (1987) to be used for a simplified description of major aspects of atmospheric circulation variability. The Climate Prediction Center (CPC) of the National Oceanic and Atmospheric Administration (NOAA) calculates a set of ten NH teleconnection patterns and associated indices on a regular basis (http://www.cpc.ncep.noaa.gov/data/teledoc/telecontents.shtml). The pattern definition is based on a rotated principal component analysis (RPCA, e.g. Hannachi et al., 2007, and references therein) applied to monthly mean standardized 500-hPa height anomalies. These ten patterns are the NAO, EA, EAWR, SCAND, POLEUR, EPNP, PNA, TNH, PT and WP (for more information see Table 1). An overview about the spatial structure of teleconnection patterns relevant for Europe can also be seen in Fig. 1 as well as for the remaining teleconnection indices on the websites of the CPC (NOAA). The associated indices are provided as monthly time series obtained from monthly mean geopotential height fields. The CPC procedure of computing patterns for individual calendar months induces a variable form of the patterns, potentially causing a different local role for the target parameter.

Additionally, the CPC provides the monthly index for the Arctic Oscillation (AO) pattern, calculated on the basis of a PCA applied to the monthly mean 1000-hPa height anomalies (http://www.cpc.ncep.noaa.gov/products/precip/CWlink/daily_ao_index/ao.shtml). Finally, we use the monthly time series of the Southern Oscillation Index (SOI) from the website of the CPC (http://www.cpc.ncep.noaa.gov/data/indices/soi), which is defined as the standardized difference between the anomalies of sea level pressure of Tahiti and Darwin.

2.2 Methods

2.2.1 Strategy

We build a multiple linear regression model for monthly mean temperature at each grid cell using the monthly indices of the above mentioned twelve patterns as predictors. Additionally we allow for a linear trend in time. As we do not expect all twelve patterns to influence the temperature in Europe during every of the considered calendar months, we select a feasible set of predictors in two steps: 1) we calculate the Pearson correlation coefficient between temperature and individual indices grid-cell-wise for each month of the year and remove all indices from the set which do not show large spatial patches of relevant correlation (cf. Fig. 2). For practical reasons, we retain a common set of predictors for all grid cells and months. 2) we select among the remaining predictors with stepwise regression based on the Akaike Information criterion (AIC) and cross-validation, in order to set up the final regression model.

2.2.2 Stepwise regression

For a given grid cell and a given month of the year, we build a linear regression model for temperature T as predictand and a set of n teleconnection indices $Z_i, i = 1, 2, 3, \ldots, n$ ($n \leq 12$) as predictors. Additionally, the time t is also considered as a predictor in order to capture

Table 1: Analysed teleconnections with associated location of centres of action during winter (except PT) including the sign of geopotential height (or pressure respectively) anomalies for their positive phases. Additionally, the active months are shown. More information is given at the website of the Climate Prediction Center (CPC) of the National Oceanic and Atmospheric Administration (NOAA) http://www.cpc.ncep.noaa.gov.

Teleconnection	Abbreviation	Centres of Action	Active Months
North Atlantic Oscillation	NAO	Greenland (-), Azores (+)	Jan.–Dec.
East Atlantic	EA	North Atlantic (-), Subtropical North Atlantic and Mediterranean (+)	Jan.–Dec.
East Atlantic/Western Russia	EAWR	NW Europe (+), Western Russia (-), NE China (+)	Jan.–Dec.
Scandinavia	SCAND	SW Europe (-), Scandinavia (+), Kazakhstan/ Mongolia (-)	Jan.–Dec.
Polar/Eurasia	POLEUR	Kara Sea (-), Mongolia (+)	Jan.–Dec.
East Pacific-North Pacific	EPNP	Eastern North America (-), Western Canada/ Alaska (+), Central North Pacific (-)	Jan.–Nov.
Pacific/North American	PNA	Hawaii (+), Western USA/ Canada (+), South Eastern US (-), Aleutian Islands (-)	Jan.–Dec.
Tropical/Northern Hemisphere	TNH	Gulf of Alaska (+), Eastern Canada (-), Gulf of Mexico/Western Atlantic (+)	Dez./Jan./Feb.
Pacific Transition	PT	Hawaii (+), Western North America (+), Gulf of Alaska (-), South Eastern US (-)	Aug./Sep.
West Pacific	WP	Kamchatka Peninsula (-), Western subtropical North Pacific/South Eastern Asia (+)	Jan.–Dec.
Arctic Oscillation	AO	Arctic (-), regions across 35–45 °N (+)	Jan.–Dec.
Southern Oscillation	SOI	Tahiti (+), Darwin (-)	Jan.–Dec.

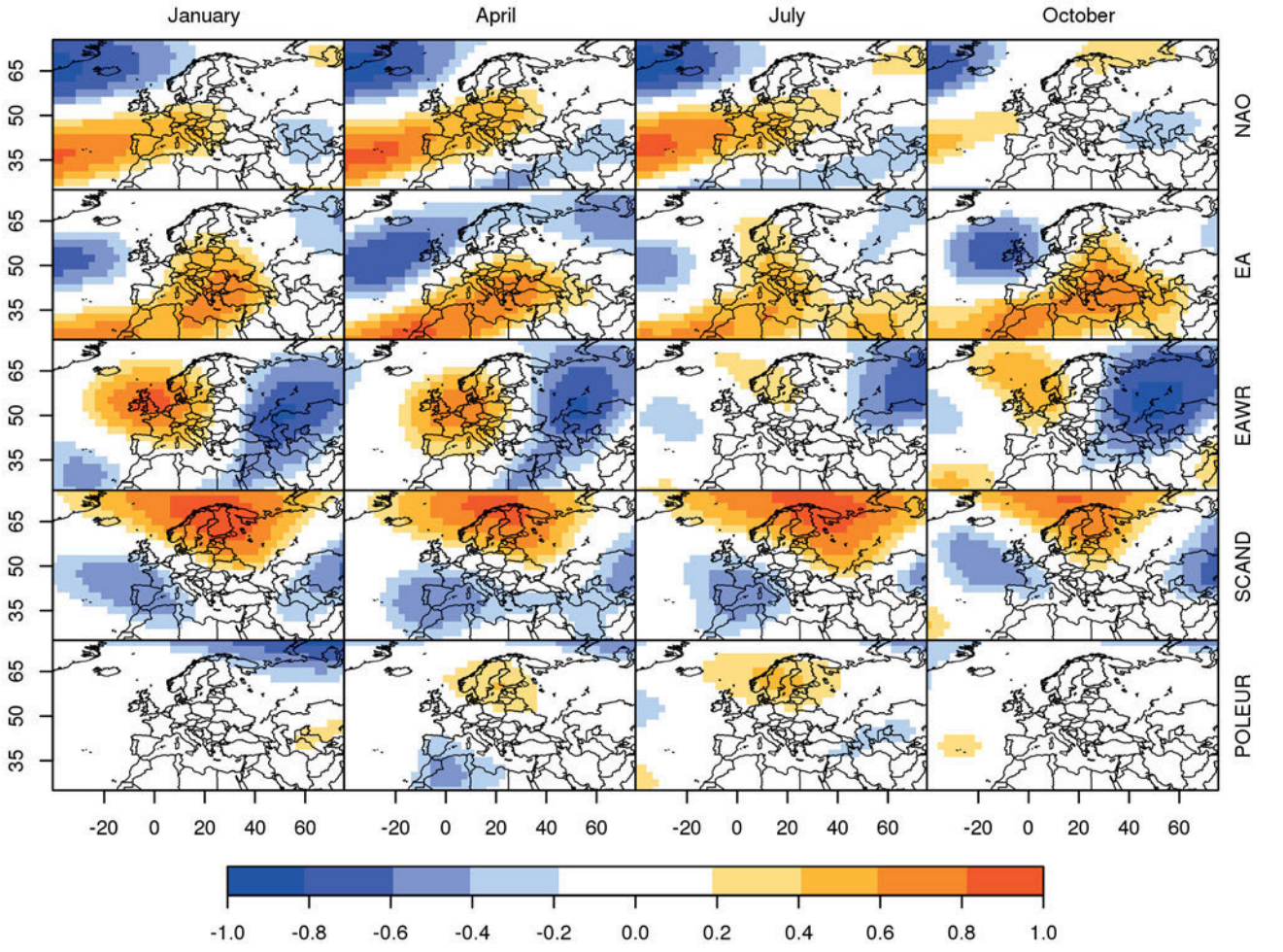

Figure 1: Pearson correlation coefficient (significant on 95 % level) between teleconnection indices and geopotential height (500-hPa) for January, April, July and October. Non significant or minor correlation coefficients (between −0.2 and 0.2) are depicted in white. Data of geopotential height from NCEP/NCAR reanalysis with resolution of 2.5 ° × 2.5 °.

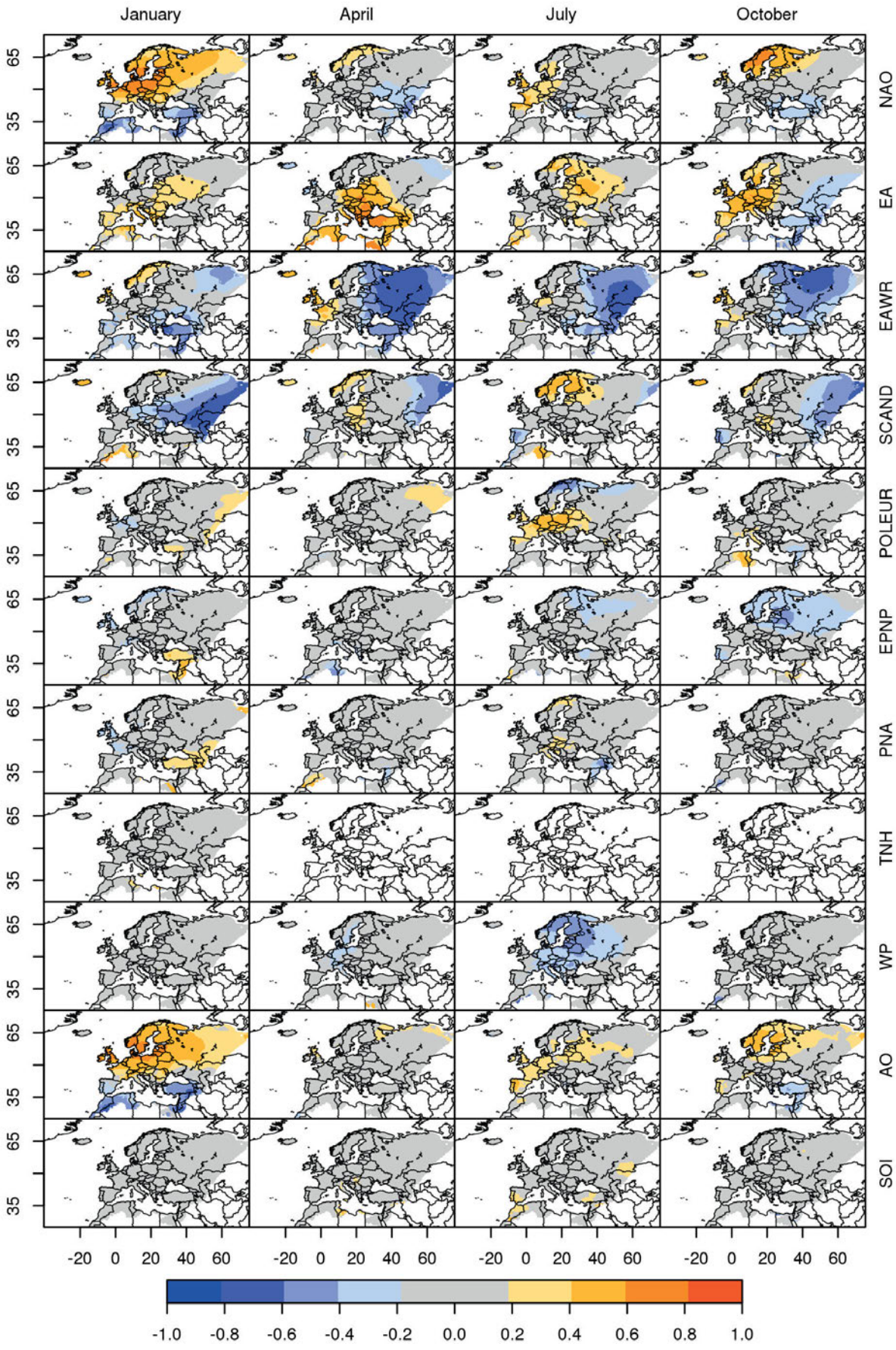

Figure 2: Pearson correlation coefficient between teleconnection indices and temperature for January, April, July and October. Non significant (5 %) or minor correlation coefficients (between −0.2 and 0.2) are depicted in grey. No data is available for white areas. PT is not active during these months and is therefore excluded.

a potential linear temperature trend in time which cannot be associated with the teleconnection indices.

$$T_j = b_0 + at_j + \sum_{i=1}^{n} b_i Z_{i,j} + \epsilon_j. \tag{2.1}$$

The index j labels different years and ϵ_j is assumed to be a series of independent normally distributed errors. Model parameters a (coefficient of the linear trend in time) and $b_i, i = 0, 1, 2, \ldots, n$ are estimated by least-squares (the function lm() in R).

Stepwise regression is an automatic procedure to select predictive variables based on a selection criterion and a well defined procedure of adding and removing predictors from the regression (e.g. Venables and Ripley, 2002; Wilks, 2011). *Forward regression* starts with none or only a few predictors and successively adds further predictors if they improve the model performance. By contrast, *backward regression* starts with the full set of predictors and successively deletes those which are not relevant for model performance. Here, we start with only the constant offset b_0 in Eq. (2.1) and seek informative predictors with stepwise-regression (function stepAIC()), allowing for both directions – forward and backward – until no further improvement can be achieved through adding or removing predictors.

Model improvement is assessed with the Akaike Information criterion (AIC, Akaike, 1974; Wilks, 2011) which, roughly speaking, measures the difference between model and observations taking the model complexity into account. For unknown variance and normally distributed errors ϵ_j the AIC is calculated by

$$\mathrm{AIC} = m \ln \left(\frac{\sum_{j=1}^{m} \epsilon_j^2}{m} \right) + 2p \tag{2.2}$$

where p labels the number of parameters and m the number of observations. We additionally evaluate the model after each regression step with a 10-fold cross-validation (e.g. Hastie et al., 2006; Wilks, 2011) by randomly dividing the data set into 10 subsets of equal size (typically 6 data points if monthly data is available for 60 years). The resulting training dataset contains 9 subsets (54 data points); the remaining subset (6 data points) is used for validation. This procedure is repeated 10 times such that each subset has been used for validation once.

The cross-validation error (CVE) is based on the mean square error (MSE) and is defined as

$$\mathrm{CVE} = \sum_{k=1}^{10} \left(\frac{n_k}{m} \right) \mathrm{MSE}_k. \tag{2.3}$$

The index k labels the 10 different groups of validation/training dataset combinations with n_k observations in the validation dataset. MSE_k is the associated mean square error of the k data group and is individually given by

$$\mathrm{MSE}_k = \frac{1}{n_k} \sum_{j_k=1}^{n_k} (T_{j_k} - \hat{T}_{j_k})^2 \tag{2.4}$$

for each data group from the cross-validation procedure, where T_{j_k} is each individual observed temperature in the k-th validation dataset and $\hat{T}_{j_k}$ is the predicted temperature estimated from the training data, i.e. all data but the k-th validation set.

Finally, if a predictor is removed due to one of these two performance indicators, this predictive variable is not present anymore in the final regression equation for a given month/grid cell.

2.2.3 Pattern-specific temperature signals

We are interested in fractions of monthly temperature anomalies caused by individual teleconnection patterns. Therefore consider the mean of the regression equation (2.1) for a given month and grid cell taken over all observed years

$$\overline{T} = a\bar{t} + \sum_{i=1}^{n} b_i \overline{Z}_i. \tag{2.5}$$

Subtracting the mean from Eq. (2.1) yields an expression for the temperature anomalies

$$T_j - \overline{T} = a(t_j - \bar{t}) + \sum_{i=1}^{n} b_i (Z_{i,j} - \overline{Z}_i) + \epsilon_j \tag{2.6}$$

describing the latter as a linear function of anomalies of the teleconnection indices. This allows to diagnose temperature anomalies associated with a specified combination of index anomalies. As the equation is linear, we can also decompose the anomaly signal into its contributions from different teleconnection patterns. These pattern-specific anomaly signals are given by

$$\mathrm{SIG}_{i,j} = b_i (Z_{i,j} - \overline{Z}_i), \tag{2.7}$$

with b_i being the individual regression coefficient and $Z_{i,j}$ the value of the teleconnection index i for a given month in a year j, $\overline{Z}_i$ is the associated long-term average for the period 1951 to 2010.

2.2.4 Model performance

The value added by using teleconnection indices in temperature forecasts based on the regression model is assessed using the mean square error skill score (MSESS) with reference to the climatological forecast (e.g. Wilks, 2011),

$$\mathrm{MSESS} = 1 - \frac{\mathrm{MSE}_{\mathrm{model}}}{\mathrm{MSE}_{\mathrm{clim}}}. \tag{2.8}$$

Similar to the model selection procedure (Section 2.2.2), we also estimate the MSESS on the basis of a 10-fold

cross-validation experiment. Improvements compared to a climatological forecast exist if the MSESS is greater than zero, a perfect forecast leads to MSESS = 1 and no improvements for MSESS ≤ 0. Although the MSESS is formally equivalent to the coefficient of determination (R^2), its value is slightly smaller as it is estimated from an out-of-sample real forecast in a cross-validation experiment.

3 Results

3.1 Predictor pre-selection

Prior to stepwise regression, we assess the linear relationship between temperature and teleconnection indices. For a given month and grid cell, we estimate the Pearson correlation coefficient and test significance with a *t*-test on a 5 % significance level. Here, a linear trend in time has been subtracted from temperature and teleconnection indices beforehand. Fig. 2 shows maps with the Pearson correlation coefficients for all teleconnection indices and the months January, April, July and October. Grid cells with non-significant correlation have been greyed out, cells with no data available are plotted in white. Restrictions in the data availability either stem from missing temperature values in the original dataset or from indices not being defined for certain months.

Notable patches of significant correlation can be found for the NAO, AO, EA, EAWR, SCAND and to a minor degree the POLEUR index. For these 6 indices, patches of similar size as well as magnitude can be found for the remaining months (not shown). Furthermore, EPNP and WP also show significant linear relationships to temperature in some regions. However, in contrast to the other 6 teleconnection patterns, large spatial links only exist for very few months (cf. Fig. 3). The remaining indices do not show a sufficiently large patch of significant correlation and will not be considered for the regression.

The box plot in Fig. 4 summarizes the monthly links between temperature and a given teleconnection index by spatially averaging the square of the correlation coefficient (r^2) for each month. Being guided by the median of the boxes, this plot supports a natural partition of teleconnection indices into two clusters which could be described as a) informative and b) non-informative for European temperature anomalies throughout the year. Cluster a) contains the five informative indices NAO, AO, EA, EAWR and SCAND. The remaining indices belong to cluster b).

Outstanding in the latter cluster are POLEUR as the most important Index in b) and TNH, which shows a notable stretch of the upper quartile towards values typically found in cluster a). Reasons for this behaviour become visible in Fig. 3 depicting the seasonal cycle of r^2. POLEUR shows only a few months (May,

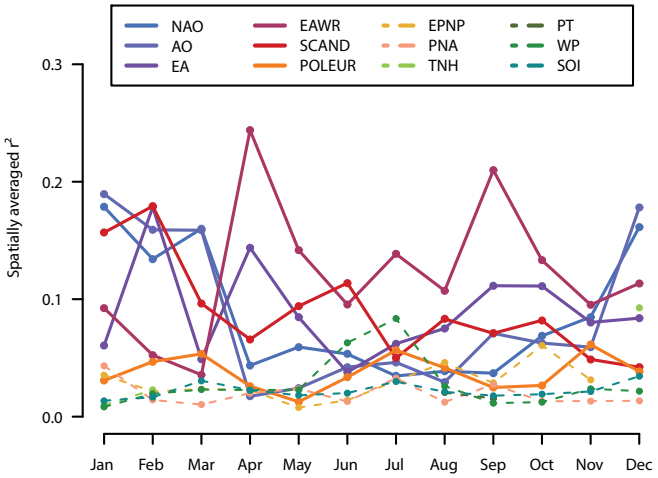

Figure 3: Spatially averaged r^2 of each teleconnection pattern for every month. Solid (dashed) lines for cluster one including POLEUR (two).

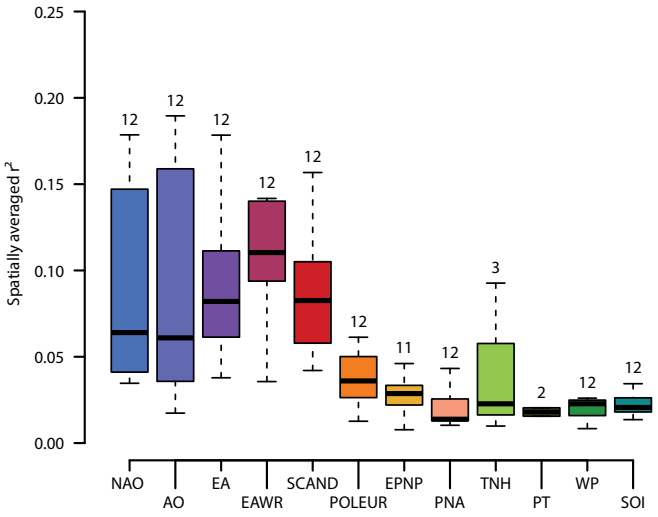

Figure 4: Spatially averaged r^2 for each teleconnection index. Boxes contain values for the available number of months denoted above each box.

September, October) with no appreciable correlation but is prominent in February, March, July and November and to a minor degree in the remaining months. TNH is only defined for winter (DJF) and shows some patches of stronger correlations in December. The mentioned links between temperature and WP (EPNP) index above, mainly occur in summer (WP) respectively from July to November (EPNP).

Aiming to include indices with notable influence on temperature in large areas of Europe and for most of the year, we choose to ignore most indices in cluster b). Hence, we build the regression model using NAO, AO, EA, EAWR and SCAND. Additionally, we include the POLEUR index as the dominant index out of cluster b) showing appreciable links to temperature in the majority of months.

Additionally to predictor selection based on their link to temperature, we investigate the mutual linear depen-

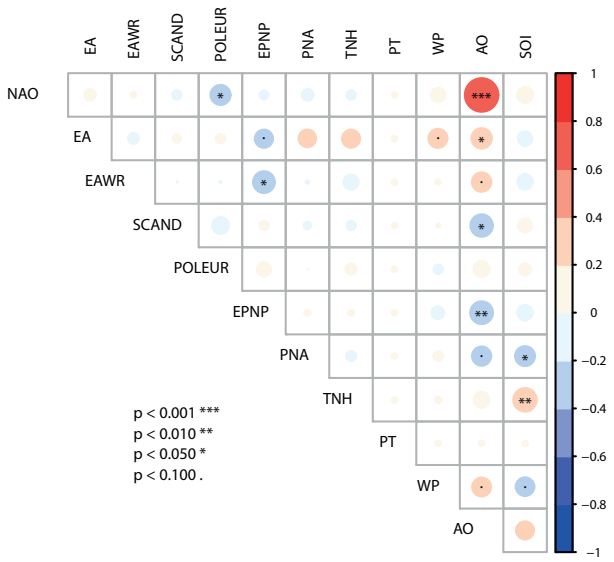

Figure 5: Pearson correlation coefficients between teleconnection indices for January. Significances are based on the t-test.

dence of the teleconnection indices by Pearson's correlation coefficient. The linear regression model will be more robust if the predictors (here the teleconnection indices) are not linearly dependent (Belsley et al., 1980). Mutual correlation of the indices for January is shown in Fig. 5. A strong linear relationship between AO and NAO is visible here and in similar pictures for the remaining months (not shown). The AO correlates weakly with other indices, such as EA, EAWR, SCAND and POLEUR. Correlations between teleconnection indices being active in the Pacific (e.g. PNA, WP) do exist as well. To avoid linear dependent predictors in the regression model, either the NAO or AO has to be dropped. Because AO also correlates with other teleconnection indices, NAO is the natural choice as predictor for stepwise regression.

3.2 Regression model

Stepwise regression as described in Section 2.2.2 is used to choose an optimal subset out of the five teleconnections indices selected in Section 3.1. Exemplarily, Fig. 6 shows the resulting regression coefficients for individual patterns for January, April, July and October. The patterns for these months are adequate representatives for the associated seasons. The remaining months have been considered as well but the coefficients are not shown. Grid cells marked grey denote that the respective index has been dropped from the optimal set during stepwise regression. Additionally, the correlations between the five teleconnection indices and the geopotential height (500-hPa) are shown in Fig. 1 for a better interpretation of links.

To verify the modelling assumptions, residuals are inspected for deviations from a normal distribution, for heteroscedasticity and for autocorrelation at various grid cells all over Europe (not shown). All assumptions are sufficiently well fulfilled.

The NAO (Fig. 6, first row) has explanatory potential for temperature in wide areas of Europe, particularly in winter; regression coefficients are positive in South Western and Central Europe, Scandinavia and northern parts of Russia. Further positive coefficients can be found for Fenno-Scandia in spring and autumn and for North Western Europe in summer. Negative coefficients are found in South Eastern Europe and parts of North Africa. Basically, coefficients magnitudes as well as the spatial dimension are larger in winter. These links between NAO and temperature are mainly influenced by circulation anomalies, which are caused by a meridional seesaw in atmospheric pressure/geopotential height between the Icelandic Low (IL) and the Azores High (AH) (e.g. Van Loon and Rogers, 1978). The advection of maritime or continental air masses dominates in winter: warmer maritime air masses are advected to Europe (except the Mediterranean) by stronger westerlies during positive NAO phase, weaker and southwards shifted westerlies associated with negative NAO phases lead to the transport of colder continental air masses by easterlies to European parts north of the Mediterranean. Due to the fact that the ocean tends to have a cooling effect on European temperatures in summer, positive regressions in North Western Europe cannot be explained by the described mechanism above. A potential mechanism is the northward shift of centres of action during summer (Mächel et al., 1998; Folland et al., 2009): for positive NAO phases, North Western Europe is now under anticyclonic influence associated with advection of continental, mostly warmer air masses from easterly parts of Europe.

Positive temperature anomalies are associated with the EA pattern (Fig. 6, second row) for large parts of Central and Western Europe. The spatial structure and extension vary with season. Basically, coefficients for Central Europe are positive throughout the year, whereas for areas surrounding Central Europe regression coefficients drop out from the model selection for several months. In winter, positive regression coefficients cover Europe except over the northern and south eastern parts; in spring northern and north western regions as well as areas in Russia are excluded. In summer (autumn) western (eastern) parts do not show positive coefficients for EA. Negative regression coefficients mainly occur during autumn and spring in the Russian regions. Due to similarities in the EA and NAO circulation patterns, European temperatures are closely connected to circulation anomalies caused by the strength of the meridional geopotential height gradient over the Atlantic. Hence influences on temperature as described for NAO mostly apply also to EA. The southerly shift of regression coefficient patterns (especially in winter/spring) compared to NAO can be explained by the south-easterly shift of

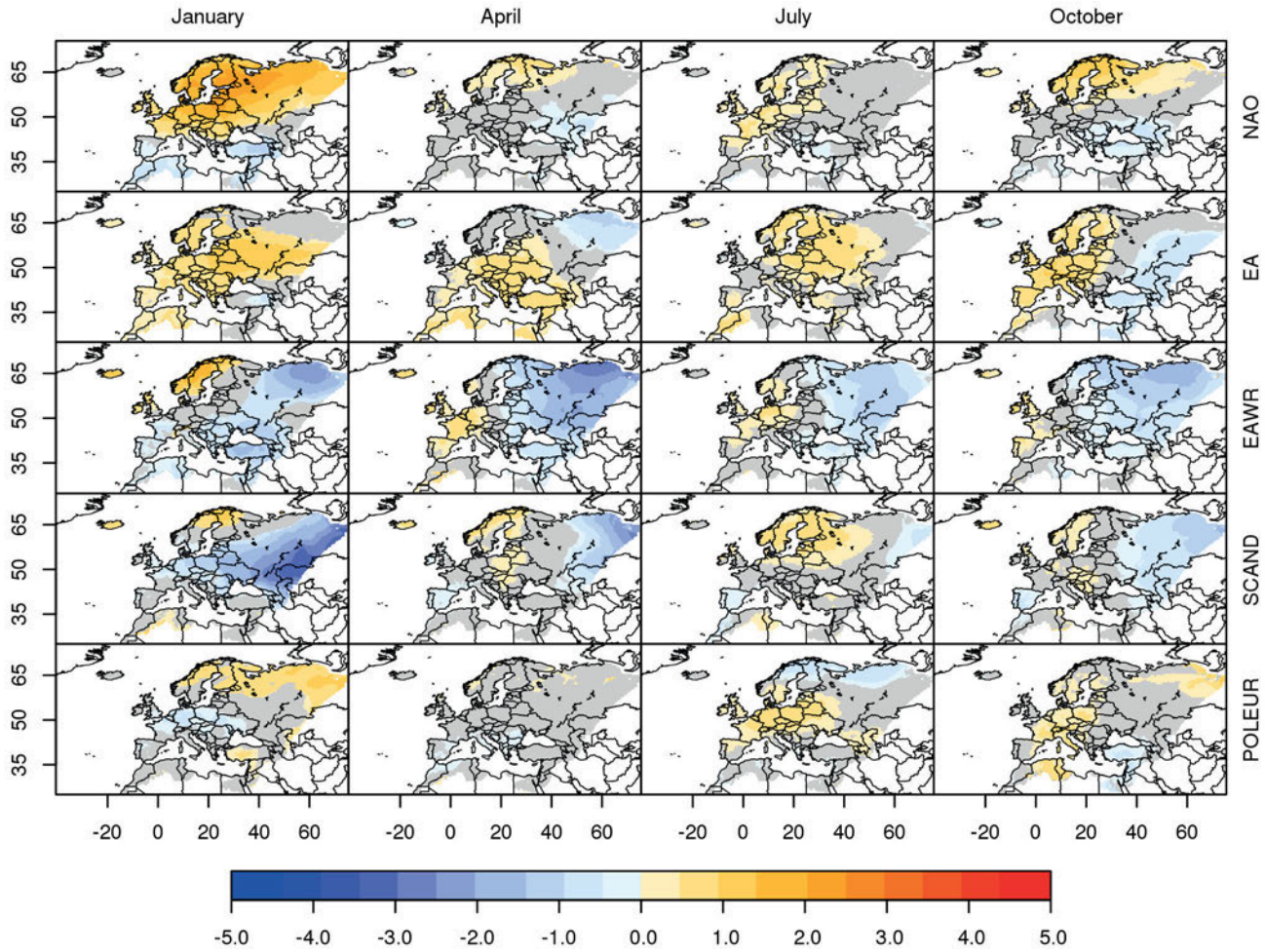

Figure 6: Regression coefficients of the monthly temperature against the teleconnection indices from a multiple linear regression for January, April, July and October. Coefficients dropped in the stepwise regression are greyed. For white grid cells, no data was available.

the EA centres of action. Additionally, the more diagonal gradient between fields of positive and negative regression coefficients (especially in autumn) is probably caused by the more zonally orientated geopotential height gradient between the EA centres of action. The similarity of the two patterns does not imply a similarity of the associated index time series (cf. correlation coefficients in Fig. 2, for more details on the characteristics of rotated PCA, we refer to Hannachi et al. (2007)).

In contrast to NAO and EA, the EAWR pattern (Fig. 6, third row) influences temperatures in parts of Fenno-Scandia and Russia/Eastern Europe, as can be seen from the extended patch of negative regression coefficients. Positive coefficients are located in Central and (North) Western Europe, however with smaller spatial extent and weaker amplitudes. These impacts on temperatures (except North Western Europe) are mainly driven by advection of northerly or southerly air masses caused by cyclonic (anticyclonic) anomalies of geopotential height in Russia (North Western Europe) during positive EAWR phases and vice versa during negative phases. Warmer temperatures in North Western Europe during winter/spring are likely to be connected to a more westerly wind component due to anticyclonic circulation (positive EAWR phase) leading to advection of relatively warm temperatures from the Atlantic.

Similar to EAWR, SCAND (Fig. 6, fourth row) plays a relevant role for temperatures in Scandinavia and Russia. A large patch of negative regression coefficients can be found from Central Europe to Russia during winter. For the remaining seasons, this large patch is complemented with smaller patches of positive coefficients in Fenno-Scandia partially extending south-eastwards (summer) and to parts of central Europe (spring), as well as small patches of weak negative coefficients in South Western and North Eastern Europe/Russia. The positive SCAND phase is closely associated to a blocking situation over the Scandinavian Peninsula, as well as with wind anomalies in 700-hPa (Bueh and Nakamura, 2007). Due to anticyclonic circulation over Scandinavia, in winter (to a minor degree in spring/autumn) cold air can be transported from Polar/Siberia regions to Eastern Europe. Warmer summer temperatures in Northern Europe are probably caused by sinking air masses related to anticyclonic circulation and associated increased solar radiation due to weaker cloud cover.

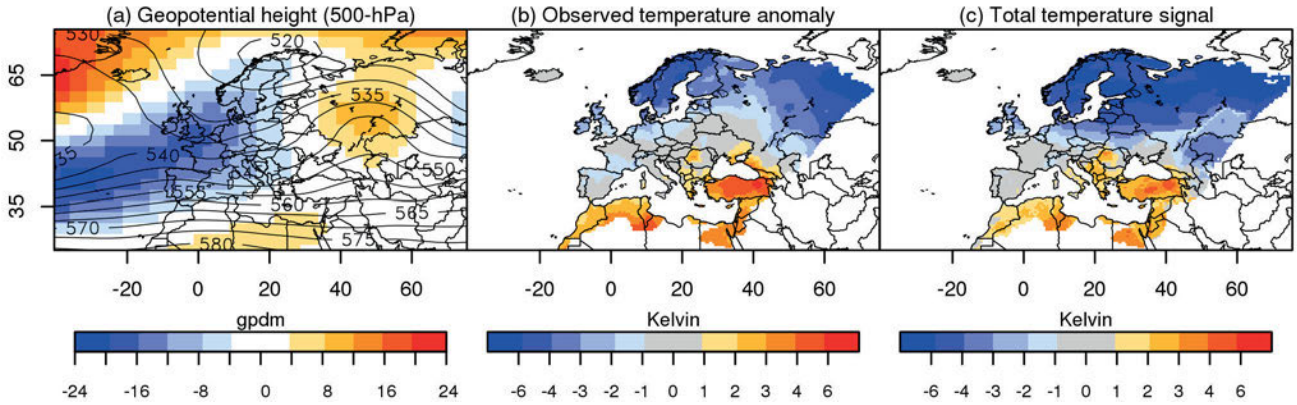

Figure 7: Geopotential height in 500-hPa (solid contour lines) and associated anomalies (shaded areas) for February 2010 in gpdm are shown in (a). Minor anomalies (between −4 and 4 gpdm) are shaded white. Data from NCEP/NCAR reanalysis (Kalnay et al., 1996) with resolution of 2.5 ° × 2.5 °. Observed temperature anomalies (b) and total temperature signal (c) on basis of five individual pattern-specific temperature signals (see Fig. 8) for February 2010 (in Kelvin). Minor anomalies (between −1 and 1 Kelvin) are depicted in grey, no data is available for white areas. All anomalies based on reference period 1981–2010.

The POLEUR pattern (Fig. 6, fifths row) has the least impact on European temperature variability and shows hardly systematic spatial structures. In winter, particularly in February and December (not shown) positive links to Fenno-Scandinavian and North Russian temperatures exist. In summer, Central European temperatures show positive coefficients for POLEUR, whereas Northern Europe shows patches of negative regressions coefficients, particular in July. Being connected to the strength of the polar vortex (Claud et al., 2007), relations to temperatures in Northern Europe can be explained by the intensified (weakened) zonal westerly flow during positive (negative) POLEUR phase leading to warmer (colder) maritime air masses being advected in winter and vice versa in summer. Positive links to Central European temperatures in summer/autumn are probably not affected directly by the polar vortex. Instead, positive correlations between geopotential height (500-hPa) and POLEUR index exist over Central Europe (Fig. 1), these are, however, not captured by the centres of action of the POLEUR pattern. The resulting anticyclonic circulation in warm months could be a reason for the temperature links.

As a corollary, it turns out that local temperatures at a given time are significantly influenced mainly by only 2 or 3 teleconnection patterns, whereas primary 1 or 2 of these are dominant. This aspect underlines the usefulness of stepwise regression with non-significant patterns ignored at individual grid cells.

Beyond the influence of teleconnections, we included a temporal component (linear trend) in the regression which has a certain descriptive power in some regions and generally shows a positive trend of approximately 0.3 K per decade in the region. As the focus is on teleconnection pattern, we do not show these coefficients here. Basically, the temporal component describes about 10–20 % of the total variance (except for regions in Northern Africa and Middle East where it describes more variance), whereas dominant teleconnection patterns (all patterns except POLEUR) account for more than 50–60 % (not shown).

3.3 Pattern-specific temperature signals

Pattern-specific contributions to monthly temperature anomalies can be deduced from the regression model using Eq. (2.5). A recent and particularly interesting case with respect to teleconnection index anomalies is February 2010. This month shows relatively large amplitudes for all relevant teleconnection indices and is used therefore to exemplify the pattern-specific signal approach. The 500-hPa field is characterised by a ridge over the North Atlantic and Greenland and an associated trough over Scandinavia and North Western Europe with a positively tilted axis (Fig. 7a). This configuration features large positive geopotential height anomalies around Greenland and negative anomalies ranging from Scandinavia south-westwards over North Western Europe to the Azores. Downstream from the Greenland ridge a weaker ridge is located over Russia. Along with this geopotential height field we find negative anomalies for NAO (−2.7), EAWR (−1.0) and POLEUR (−1.9) and positive anomalies for EA (1.2) and SCAND (1.0).

The pattern-specific contribution to temperature anomalies depends on the associated teleconnection index anomaly and the related regression coefficient. The estimated pattern-specific temperature signals are depicted in Fig. 8.

A strong negative anomaly of the NAO index is associated with a large patch of negative temperature anomalies, ranging from South Western Europe (−1 K) to Fenno-Scandia and Northern Russia (up to −5 K). Patches of positive temperature anomalies can be found in Northern Africa and South Eastern Europe (1–4 K). The EA pattern is associated with mostly warmer temperatures in Europe (1–3 K) except the northernmost

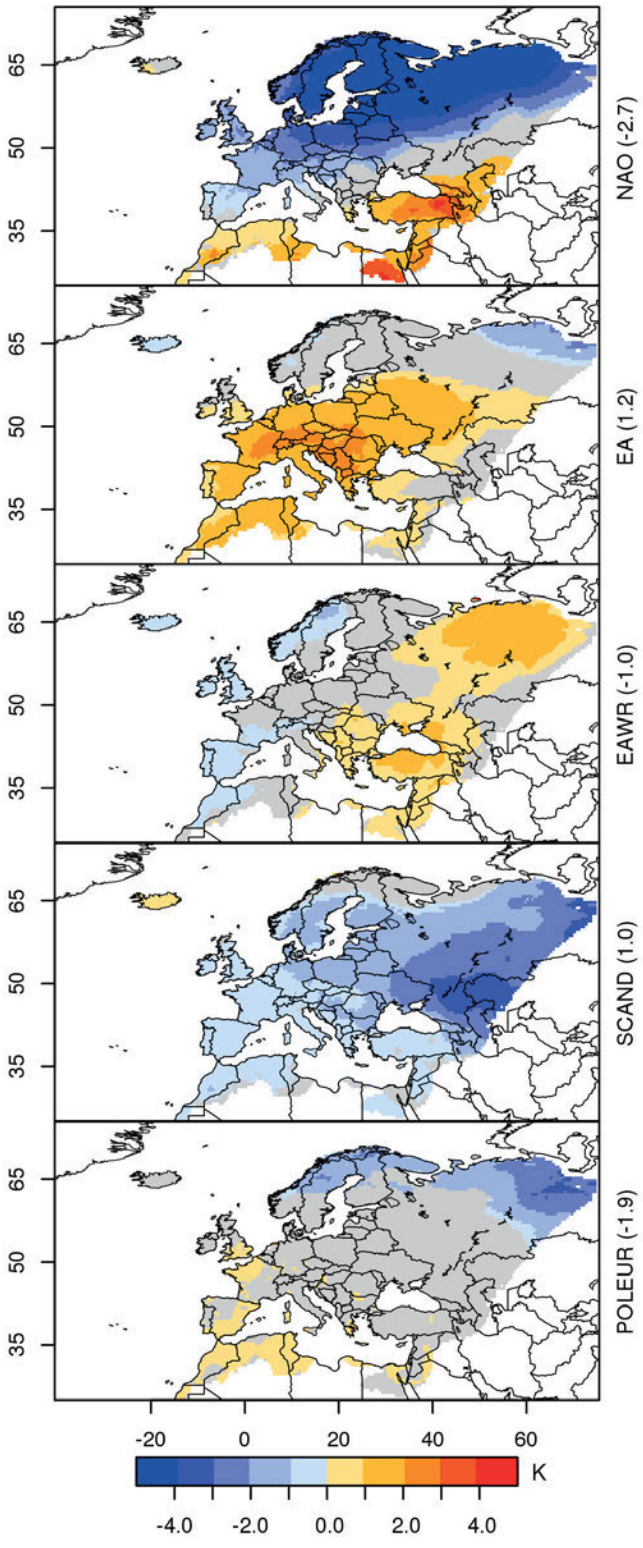

Figure 8: Modelled pattern-specific temperature signals (in Kelvin) for February 2010. No signals due to associated coefficients dropped in the stepwise regression are depicted in grey. No data available for white areas. In addition, index anomalies are displayed on the right side.

part. Temperature signals linked to EAWR are weaker; north eastern and south eastern parts of Europe exhibit patches of positive temperature anomalies (up to 2 K) and westerly regions (Spain, parts of the UK and Norway) show slightly negative anomalies (mainly −1 K). The negative anomaly of SCAND is associated with colder temperatures in wide areas of Europe (except Northern Europe and Iceland) with a gradient from east (−4 K) to west (−1 K). Negative temperature anomalies (up to −3 K) in the northern part of Northern Europe are linked to a negative anomaly of the POLEUR index.

Fig. 7c shows the total temperature signal resulting from summing up the 5 pattern-specific signals. Particularly the anomalies of NAO, SCAND and POLEUR lead to colder temperatures (up to −6 K) in northern parts of Europe ranging from Great Britain and Germany to Ukraine. Warmer temperatures up to 4 Kelvin can be expected in South Eastern Europe and Northern Africa mainly by anomalies of NAO, EA and EAWR. Rarely temperature variations exist in parts of Central and Western Europe due to opposite contributions of NAO and EA in these regions. This interplay between NAO and EA and its impact on European winter temperatures is also discussed in Moore and Renfrew (2012). Basically, the spatial structure and tendencies of the modelled anomalies caused by teleconnection patterns correspond with observed temperature anomalies (Fig. 7b). Especially, the meridional dichotomy is captured, although there are differences in amplitude. Even the modelling of total temperature signal in the Baltic, North Western Russia and parts of Scandinavia is too cold.

3.4 Model performance

We assess the performance of the regression model by comparing the model forecast based on the teleconnection indices to a climatological forecast using the MSESS (Section 2.2.4). The MSESS has been obtained from a cross validation experiment described in Section 2.2.2. Fig. 9 shows the resulting skill score for every month.

The skill score is basically positive over the full region and all months, indicating added value of the regression model over the climatological forecast. Quantitatively, the positive skill varies regionally and with season. Up to 80 % decrease in MSE compared to the climatological forecast can be obtained for example for Spain and the Maghreb in February or for parts of Russia in May, September and October. Less than 20 % of error reduction is possible, e.g. in Fenno-Scandia and Western Europe in spring and Eastern Europe in October. Spacious regions with no improvement (grey areas) can be found, e.g. from Poland to the Black Sea in June or in parts of Egypt during several months (e.g. January and July). These areas are often characterised by a model configuration, which only includes the constant offset as predictor. However, on average in wide regions (e.g. Central and Western Europe, Russia, Scandinavia)

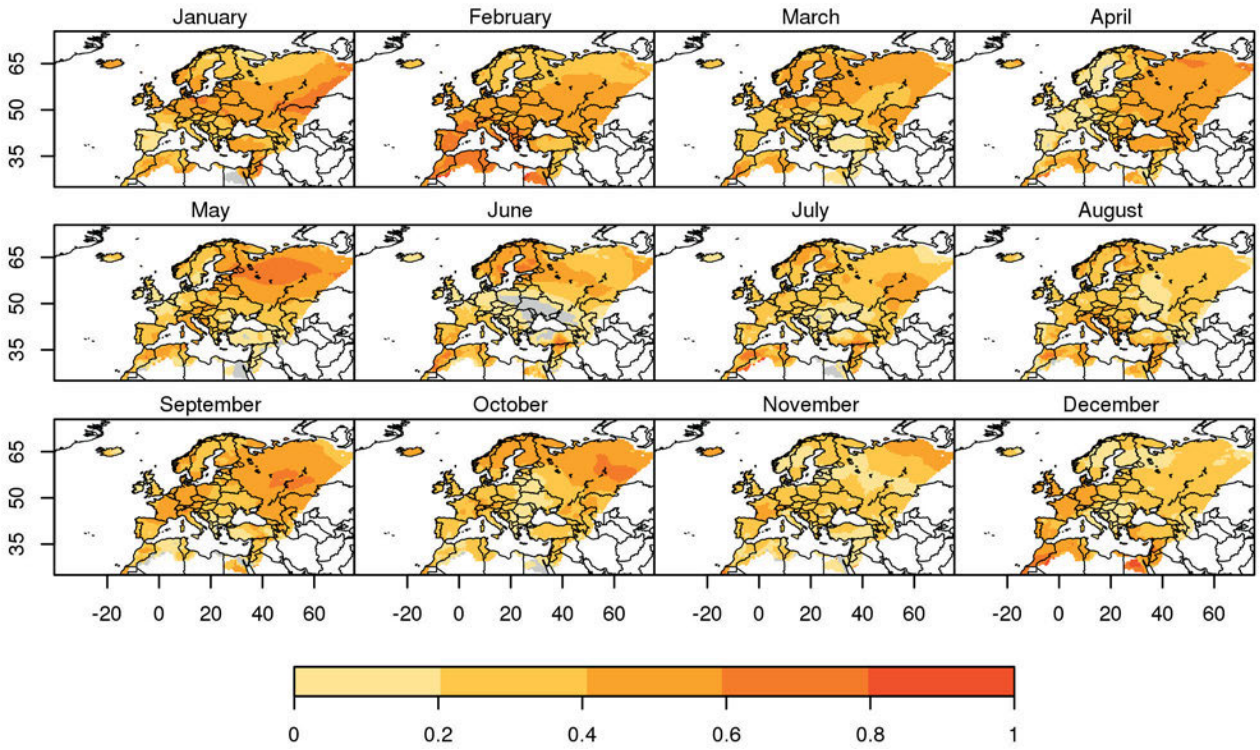

Figure 9: Monthly skill score based on cross-validation error of the models (compared to 1951–2010 climatology). Negative values are depicted in grey. No data is available for white areas.

improvements of 20–60 % can be obtained for most of the months.

A spatially averaged skill score for each month is depicted in Fig. 10. The model exhibits its strength at the beginning of the year with about 40 % skill and decays towards summer to 30 %. September and October are slightly better and for November and December, the model is back to about its summer performance. Fig. 9 discloses Eastern Europe and the Black Sea regions responsible for the low summer skill; November and December show low skill for Fenno-Scandia and associated regions to the east. Most skill is obtained in Russian regions during spring/autumn months, where especially the EAWR pattern has the most influence (see Section 3.2). During these seasons the meridional temperature gradient between polar and subtropical regions is very high and different air masses driven by the EAWR phase (associated with northerly/southerly winds) can strongly influence the temperature in Russia. Hence, variations of the EAWR index are closely connected to temperature variabilities with intense signals.

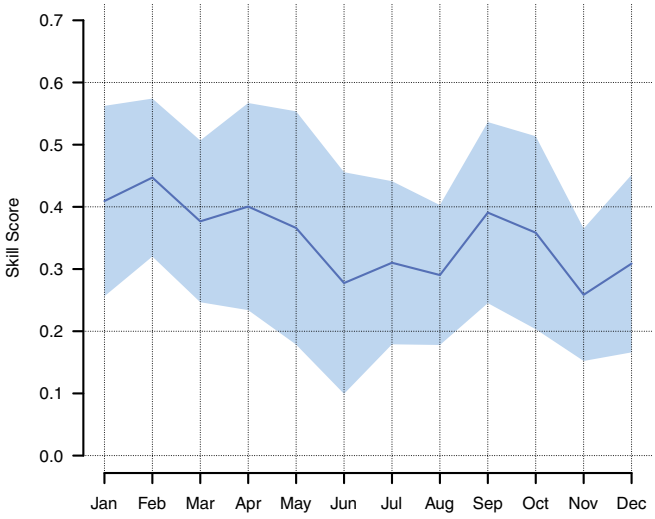

Figure 10: Spatially averaged skill score for each month (blue line). Shaded areas mark ±1 standard deviation of the spatially distributed values.

4 Summary and discussion

We investigate links between European temperature anomalies and the indices capturing the variability of large-scale atmospheric NH teleconnection patterns. An exploratory correlation analysis reveals a subset of indices being relevant here. For this subset, we build multiple linear regression models for temperature anomalies at each grid cell. As predictors we include NAO, EA, EAWR, SCAND and POLEUR indices in addition to a linear trend in time. Stepwise regression based on AIC and a cross-validation error is used to select predictors relevant for the grid cell at hand.

The resulting spatial patterns of regression coefficients associated with a circulation pattern are discussed. Except POLEUR, each of the remaining atmo-

spheric teleconnection patterns has a notable influence on European temperatures in most regions and months. However, there exist spatial and seasonal differences among the patterns. NAO and EA particularly affect wide areas in Northern, Western, Central and South Western Europe. In contrast, the EAWR pattern has an dominant impact on temperatures in Fenno-Scandia, Russia and Eastern Europe. SCAND affects similar regions, but besides Scandinavia and Russia, temperatures in South Western Europe are also linked to the SCAND pattern. POLEUR shows weaker influences on temperature, less structured and with smaller contiguous patches, especially in Fenno-Scandia (winter) and Central Europe (summer). These spatial configurations of influences associated to the teleconnection patterns are in good agreement with other studies mentioned in the introduction.

Local temperatures are significantly influenced mainly by only 2 to 3 teleconnection patterns at the same time, whereas primary 1 or 2 atmospheric patterns are dominant. From a 10-fold cross-validation, we estimate a 30 % to 40 % improvement in forecasting temperature anomalies for the regression model built here with respect to a climatological forecast. Improvements are stronger in winter and spring; strong improvements can be found in Russian regions, whereas areas around the Black Sea as well as in Western Europe have least improvements. Seasonal and spatial variations might be mainly caused by different synoptic situations depending on region and season. More temperature variability due to a more frequent alternation of the influence of either maritime or continental air masses could be a reason for a better performance in eastern parts of Europe (except areas around the Black Sea, see Section 3.4) than parts in mostly maritime affected western Europe. Smaller synoptic systems (Rudeva and Gulev, 2007) and generally reduced synoptic dynamic processes in warmer months affecting the temperature variability is a possible explanation for the performance being worse in summer. Additionally, blocking effects (e.g. Lejenäs and Økland, 1983) with strongly associated temperature anomalies and, of course, their associated variabilities are more dominant in winter and spring.

From the regression model, we deduce temperature anomaly signals associated with anomalies of a given teleconnection index. These signals allow to assess spatial patterns of temperature anomalies due to a given index anomaly. As they stem from a linear model, individual signals can be superposed to obtain an aggregated signal. This can serve as an educated first guess of local temperature forecasts given the characteristics of large scale circulation in the form of teleconnection indices, useful for climate monitoring, seasonal forecasts and climate projection downscaling. The principle is demonstrated exemplarily with the situation found for February 2010. This month is characterised by moderate to strong index anomalies of their associated large-scale patterns. The aggregated temperature signal (without the temporal component) is already in a good agreement with observed anomalies except for the Baltic region, Belarus and Western Russia. The model is linear in the response to teleconnection patterns and is not able to capture non-linear or micro-scale effects. Aside from these teleconnection patterns, other large-scale influences on climate (among others European temperatures) exist, for instance, the sea ice extent (e.g. Petoukhov and Semenov, 2010), snow cover (e.g. Wagner, 1973; Leathers et al., 1995), sea surface temperature in the Atlantic Ocean (e.g. Czaja and Frankignoul, 1999; Sutton and Hodson, 2005), as well as the Mediterranean Sea (e.g. Sun and Yuan, 2009). The influence of these factors can be only partially captured by the linear trend in time which is included in the models; they furthermore interact with the large-scale atmospheric circulation patterns. Nevertheless, it is quite surprising that a relatively simple linear regression model proves this useful for modelling European temperature anomalies.

A straight-forward improvement would be to build a seasonal and spatial model instead of individual regression models for every month and grid cell. In this way, strength can be borrowed from neighbouring months and grid cells; the number of parameters will be reduced and the model will be more robust. However, despite these possible extension, the model presented here provides a sound basis for forecasting and monitoring European temperatures influenced by large-scale circulation patterns.

Acknowledgments

The authors are grateful to two anonymous reviewers for very constructive comments! We acknowledge the availability of the E-OBS dataset from the EU-FP6 project ENSEMBLES (http://ensembles-eu.metoffice.com), the data providers for the ECA&D project (http://www.ecad.eu) and the Climate Prediction Center (CPC) of the US National Oceanic Atmospheric Administration (NOAA) for providing the teleconnection indices, as well as the NOAA-ESRL Physical Sciences Division, Boulder Colorado for making available the NCEP-NCAR reanalysis geopotential height dataset.

References

Akaike, H., 1974: A new look at statistical model identification. – IEEE Transactions on Automatic Control **AC-19**, 716–722.

Barnston, A.G., R.E. Livezey, 1987: Classification, seasonality and persistence of low-frequency atmospheric circulation patterns. – Mon. Wea. Rev. **115**, 1083–1126.

Belsley, D.A., E. Kuh, R.E. Welsch, 1980: Regression Diagnostics–Identifying Influential Data and Sources of Collinearity. – John Wiley and Sons, New York.

Bueh, C., H. Nakamura, 2007: Scandinavian pattern and its climatic impact. – Quart. J. Roy. Meteor. Soc. **133**, 2117–2131.

Claud, C., B. Duchiron, P. Terray, 2007: Associations between large-scale atmospheric circulation and polar low developments over the North Atlantic during winter. – J. Geophys. Res. **112**, D12101.

Czaja, A., C. Frankignoul, 1999: Influence of the North Atlantic SST on the atmospheric circulation. – Geophys. Res. Lett. **26**, 2969–2972.

Folland, C.K., J. Knight, H.W. Linderholm, D. Fereday, S. Ineson, J.W. Hurrell, 2009: The Summer North Atlantic Oscillation: Past, Present, and Future. – J. Climate **22**, 1082–1103.

Fraedrich, K., 1994: An ENSO impact on Europe? – Tellus **46A**, 541–552.

Halpert, M.S., C.F. Ropelewski, 1992: Surface Temperature Patterns Associated with the Southern Oscillation. – J. Climate **5**, 577–593.

Hannachi, A., I.T. Jolliffe, D.B. Stephenson, 2007: Empirical orthogonal functions and related techniques in atmospheric science: A review. – Int. J. Climatol. **27**(9), 1119–1152.

Hastie, T., R. Tibshirani, J. Friedman, J. Franklin, 2006: The elements of statistical learning: data mining, inference and prediction. – The Mathematical Intelligencer **27**, 83–85.

Haylock, M.R., N. Hofstra, A.M.G. Klein Tank, E.J. Klok, P.D. Jones, M. New, 2008: A European daily high-resolution gridded dataset of surface temperature and precipitation. – J. Geophys. Res. Atmos. **113**, 1–12.

Hurrel, J.W., 1995: Decadal Trends in the North Atlantic Oscillation: Regional Temperatures and Precipitation. – Science **269**, 676–679.

Hurrell, J.W., C. Deser, 2009: North Atlantic climate variability: The role of the North Atlantic Oscillation. – J. Mar. Syst. **78**, 28–41.

Kalnay, E., M. Kanamitsu, R. Kistler, W. Collins, D. Deaven, L. Gandin, M. Iredell, S. Saha, G. White, J. Woollen, Y. Zhu, A. Leetmaa, R. Reynolds, M. Chelliah, W. Ebisuzaki, W. Higgins, J. Janowiak, K.C. Mo, C. Ropelewski, J. Wang, R. Jenne, D. Joseph, 1996: The NCEP/NCAR 40-Year Reanalysis Project. – Bull. Amer. Meteor. Soc. **77**, 437–470.

Knippertz, P., U. Ulbrich, F. Marques, J. Corte-Real, 2003: Decadal changes in the link between El Niño and springtime North Atlantic Oscillation and European–North African rainfall. – Int. J. Climatol. **23**, 1293–1311.

Kutiel, H., Y. Benaroch, 2002: North Sea–Caspian Pattern (NCP) – an upper level atmospheric teleconnection affecting the eastern Mediterranean: Identification and definition. – Theor. Appl. Climatol. **71**, 17–28.

Kutiel, H., P. Maheras, M. Türkeş, S. Paz, 2002: North Sea–Caspian Pattern (NCP) – an upper level atmospheric teleconnection affecting the eastern Mediterranean - implications on the regional climate. – Theor. Appl. Climatol. **72**, 173–192.

Leathers, D.J., A.W. Ellis, D.A. Robinson, 1995: Characteristics of temperature depressions associated with snow cover across the northeast United States. – J. Appl. Meteorol. **34**, 381–390.

Lejenäs, H., H. Økland, 1983: Characteristics of northern hemisphere blocking as determined from a long time series of observational data. – Tellus **35A**, 350–362.

Mächel, H., A. Kapala, H. Flohn, 1998: Behaviour of the centres of action above the Atlantic since 1881. Part I: Characteristics of seasonal and interannual variability. – Int. J. Climatol. **18**, 1–22.

Maraun, D., H.W. Rust, T.J. Osborn, 2012: The influence of synoptic airflow on UK daily precipitation extremes. Part II: regional climate model and e-obs data validation. – Climate Dyn. **39**, 287–301.

Moore, G.W.K., I.A. Renfrew, 2012: Cold European winters: interplay between the NAO and the East Atlantic mode. – Atmos. Sci. Lett. **13**, 1–8.

Nissen, K.M., G.C. Leckebusch, J.G. Pinto, D. Renggli, S. Ulbrich, U. Ulbrich, 2010: Cyclones causing wind storms in the mediterranean: characteristics, trends and links to large-scale patterns. – Nat. Haz. Earth Sys. Sci. **10**, 1379–1391.

Petoukhov, V., V.A. Semenov, 2010: A link between reduced Barents-Kara sea ice and cold winter extremes over northern continents. – J. Geophys. Res. **15**, D21111.

Pozo-Vázquez, D., M.J. Esteban-Parra, F.S. Rodrigo, Y. Castro-Díez, 2001: The Association between ENSO and Winter Atmospheric Circulation and Temperature in the North Atlantic Region. – J. Climate **14**, 3408–3420.

Rudeva, I., S.K. Gulev, 2007: Climatology of Cyclone Size Characteristics and Their Changes during the Cyclone Life Cycle. – Mon. Wea. Rev. **135**, 2568–2587.

Sun, J., W. Yuan, 2009: Contribution of the Sea Surface Temperature over the Mediterranean-Black Sea to the Decadal Shift of the Summer North Atlantic Oscillation. – Adv. Atmos. Sci. **26**, 717–726.

Sutton, R.T., D.L.R. Hodson, 2005: Atlantic Ocean Forcing of North American and European Summer Climate. – Science **309**, 115–118.

Thompson, D.W.J., J.M. Wallace, 1998: The Arctic Oscillation signature in the wintertime geopotential height and temperature fields. – Geophys. Res. Lett. **25**, 1297–1300.

Ulbrich, U., P. Lionello, D. Belušic, J. Jacobeit,, P. Knippertz, F.G. Kuglitsch, G.C. Leckebusch, J. Luterbacher, M. Maugeri, P. Maheras, others, 2012: Climate of the mediterranean: synoptic patterns, temperature, precipitation, winds, and their extremes. – In: Lionello, P. (Ed.): The climate of the mediterranean region from the past to the future. – Elsevier, 301–346.

Van Loon, H., J.C. Rogers, 1978: The Seesaw in Winter Temperatures between Greenland and Northern Europe. Part I: General Description. – Mon. Wea. Rev. **106**, 296–310.

Van Oldenborgh, G.J., G. Burgers, A.K. Tank, 2000: On the El Niño teleconnection to spring precipitation in Europe. – Int. J. Climatol. **20**, 565–574.

Venables, W.N., B.D. Ripley, 2002: Modern Applied Statistics with S. – Springer-Verlag, New York.

Wagner, A.J., 1973: The influence of average snow depth on monthly mean temperature anomaly. – Mon. Wea. Rev. **101**, 624–626.

Walker, G.T., E.W. Bliss, 1932: World Weather V. – Mem. R. Meteor. Soc. **4**, 53–84.

Wilks, D.S., 2011: Statistical methods in the atmospheric sciences. – Academic Press, San Diego, CA.